A 3D-CFD numerical framework for the simulation of both light- and heavy-duty Diesel injectors

Simone Sparacino[1*], *Massimo* Borghi[1]

[1]Department of Engineering "Enzo Ferrari", University of Modena and Reggio Emilia, Via Vivarelli 10, Modena 41125, Italy

Abstract. In spite of the effort of the engine manufacturers to improve exhaust aftertreatment efficiency, thus reducing tailpipe pollutants, the unaffordable tightening of the laws dealing with emissions puts a strain on the use of Diesel engines for passenger cars in the next decades. However, for trucks and marine applications, such technology may remain the predominant solution all over the world. For this reason, development of heavy-duty Diesel engines goes on and Computational Fluid Dynamics (CFD) can play a crucial role in supporting designers. Among the different goals of the numerical analyses on Diesel engines, 3D-CFD Lagrangian simulations can be adopted to optimize fuel injection, which is a crucial aspects as able to affect both combustion efficiency and emissions. For this purpose, a robust numerical framework is needed. The present work aims at proving that models suitable for the simulation of light-duty Diesel injectors can be proficiently extended for heavy-duty ones. In particular, attention is here focused on droplet break-up. An alternative secondary break-up model is proposed. It is purposely calibrated on the well-known Spray A injector provided by the Engine Combustion Network (ECN), which can be assumed as representative of injectors for light-duty applications. 3D-CFD simulations are validated against experimental data in terms of both liquid and vapour penetrations and imaging. Then, the numerical set-up adopted for the Spray A is employed without any further ad-hoc tuning to investigate Spray C and Spray D which can be considered, instead, representative of heavy-duty nozzles. The proposed model proves to be effective for the prediction of the break-up rate. All the injectors are tested via vessel simulations characterized by the same ambient pressure and temperature, equal to 6 MPa and 900 K respectively. Even the adopted fuel is common, namely n-Dodecane, whose injection pressure and temperature are fixed to 150 MPa and 363 K, respectively.

[*1] Corresponding author: simone.sparacino@unimore.it

1 Introduction

The complexity of both gasoline and Diesel engines has rapidly increased in the last years, in order to increase the efficiency and reduce the emissions. As for spark-ignition (SI) powertrains, such targets are currently achieved via different techniques such as downsizing, turbocharging, Gasoline Direct Injection (GDI), complex fuel injection strategies, variable valve timing, alternative ignition technologies [1] and water injection [2]. As for compression-ignition (CI) engines, main strategies to reduce the specific fuel consumption is the joint optimization of piston bowl and injection parameters [3] and the reduction of gas-to-wall heat losses by means of thermal barrier coatings. In addition, there are techniques that are shared by the two engine categories or even allow to blend the same. In fact, hybridization is currently proposed for both gasoline and Diesel engines [4-6]. Moreover, innovative combustions, such as HCCI or GCI [7, 8], represent a mix that allows to take advantage of the positives of both the engine types.
Despite the really complex scenario, the noticeable efforts by manufacturers may not be sufficient to ensure the survival of the Diesel engine to power on road vehicles, at least the light-duty ones such as passenger-cars. However, in the light of the huge powers as a consequence of the noticeable involved masses, Diesel will likely remain the predominant solution for trucks and marine applications.
Therefore, Computational Fluid Dynamics (CFD) can go on in supporting CI engine development towards a massive reduction of tailpipe emissions. In the last years, the number of CFD applications on both SI and CI engines aiming at make the design faster has rapidly increased. Currently, 0D chemical reactor calculations can estimate Laminar Flame Speed (LFS) [9], gas precursors of Soot [10, 11] and Auto-Ignition (AI) delays [12], which can help to predict start of combustion in CI engines or knock in SI ones. 1D tools can define the engine layout since the early stage of design thanks to the improved predictive capabilities [13-16]. Detailed 3D analyses can prevent abnormal combustions [17, 18] and thermo-mechanical failures [19-22] in current production highly-downsized SI engines. Alternatively they can evaluate the effect of turbulence (via complex approaches and dedicated post-processing techniques) [23-27], the impact of alternative valve actuation strategies [28], the efficiency of innovative combustions [29], the contribution of turbulent jet ignition (TJI) [30] and the advantage of water injection [31-33]. Moreover, 3D tools can virtually test alternative cooling techniques [34] or insulating coatings [35] and, mostly for Diesel engines, they can optimize both the combustion chamber geometry and the injection strategy [36-38] to simultaneously increase combustion efficiency and reduce emission production.
Focusing on the injection optimization for CI engines, a robust numerical spray representation is needed. The most widespread approach for fuel injection simulations is the Arbitrary Lagrangian-Eulerian (ALE) one, thanks to its computational efficiency. It relies on several models to describe the spatial and temporal evolution of the injected fuel, such as the one describing the secondary break-up. The latter is of primary importance in Diesel engines. In fact the high back-pressure available in the cylinder leads to a very rapid phenomenon of droplet disruption. Several models are available in literature for the 3D-CFD simulation of secondary break-up. A detailed review of the most popular ones, such as the Reitz-Diwakar and the KHRT, can be found in [39]. Each of them models the disruption of computational parcels due to aerodynamic forces at the liquid-air interface and it is characterized by constants (calibrated on experimental evidence) which can be exploited for tuning.
An alternative secondary break-up model, hereafter briefly indicated as “GruMo”, is proposed in the present paper. The model aims at minimizing secondary break-up

calibration efforts in ALE simulations of Diesel sprays. For this goal, a zonalization of the break-up regimes is introduced. Specifically, near the nozzle, where gas Weber number is high, only stripping break-up is enabled. Conversely, sufficiently far from it, only bag break-up mechanism is accounted for. Firstly, the "GruMo" model is properly calibrated against experimental data on the well-known Spray A injector provided by the ECN, whose geometric hole and mass flow rate can be considered as representative for light-duty application injectors. Then, without any further dedicated tuning, the model is adopted to simulate both Spray C and Spray D still provided by the ECN. The numerical-experimental comparison reveals that the GruMo model is able to properly predict droplet break-up even for these injectors, whose characteristics are typical of heavy-duty applications. This demonstrates that the proposed numerical framework can be proficiently adopted to simulate both light- and heavy-duty nozzles.
Moreover, the proposed approach is systematically compared with the most diffused model in the engine community for spray Diesel simulation, namely the Reitz-Diwakar [40, 41].
The structure of the paper is briefly recalled. Firstly, the new GruMo break-up model is discussed in-depth. Secondly, available experimental data, investigated operating condition and numerical setup are presented. Thirdly, results are discussed in details. Finally, conclusions on the activity are drawn.

2 The proposed GruMo break-up model

Secondary break-up is the disruption of a liquid droplet into smaller ones caused by aerodynamic forces due the relative velocity between droplet and surrounding gas. Surface tension force opposes to deformation and, thus, to break-up, trying to keep the droplet spherical. Such competition can be formalized introducing the dimensionless gas phase Weber number reported in Eq. 1, which represents the ratio between aerodynamic force and surface tension. v_{rel} represents the relative velocity between droplet and gas and it is defined as in Eq. 2 where u, v, w and u_d, v_d, w_d are velocity components of gas and droplet in the global coordinate system, respectively. r_d and D_d are droplet radius and diameter, ρ_{gas} is the density of the surrounding gas, and σ_d is the liquid surface tension.

$$We_g = \frac{v_{rel}^2 \, r_d \, \rho_{gas}}{\sigma_d} = \frac{v_{rel}^2 \, D_d \, \rho_{gas}}{2\sigma_d} \quad (1)$$

$$v_{rel} = \sqrt{(u-u_d)^2 + (v-v_d)^2 + (w-w_d)^2} \quad (2)$$

From experimental investigations it is known that, based on the gas Weber number, different droplet break-up mechanisms exist. Following criteria proposed by Pilch and Erdman [42], Vibrational, Bag, Bag-Streamer, Stripping and Catastrophic mechanisms occur for $We_g \leq 12$, $12 < We_g \leq 50$, $50 < We_g \leq 100$, $100 < We_g \leq 350$ and $We_g > 350$, respectively. At engine-like conditions, all the described break-up mechanisms can occur. However, the disintegration process mainly takes place near the nozzle where the Weber number is remarkably high.
Existing and most diffused secondary break-up models for gasoline and Diesel sprays do not account for all the mechanisms mentioned above. For example, the Reitz-Diwakar only considers bag and stripping.
The GruMo break-up model is similar to the Reitz-Diwakar one but, compared to the latter, it splits the computational domain in two zones, separated by a "transition distance" T_d, equal to 8 mm. According to [41, 43], stripping is assumed near the nozzle, where We_g is higher, while Bag is accounted for downstream T_d. The reason for this separation is purely empirical. It is, de facto, just a numerical expedient to simplify the calibration process. In

fact traditional models are characterized by a continuous competition between the mechanisms everywhere in the domain. In other words, each break-up regime can occur everywhere in the domain and the predominant one is determined, per each droplet, based on the local conditions affecting both Weber number and characteristic break-up times. Therefore, it is not possible to determine a priori which type of mechanism a droplet is experiencing. Conversely, via zonalization, identification of the governing break-up mechanism is straightforward, as it simply depends on the droplet position in the injection domain. This allows a much faster calibration of the model parameters.
In addition, the separation will be exploited in a future work to formulate simple correlation functions between model parameters and operating conditions. In fact, the ultimate goal will be to transform Reitz-Diwakar model constants into variable parameters, dependent on ambient conditions and injection parameters. In fact, as it will be evident in the results section, traditional models are not able to provide a reliable estimation of the break-up rate at any condition without ad-hoc calibration of the constants.
For the GruMo model implementation, the first quantity to be defined is the distance of each droplet from the nozzle, which is evaluated as in Eq. 3.

$$\mathrm{DIST_{inj}} = \sqrt{\left(\mathrm{x_{inj}} - \mathrm{x_d}\right)^2 + \left(\mathrm{y_{inj}} - \mathrm{y_d}\right)^2 + \left(\mathrm{z_{inj}} - \mathrm{z_d}\right)^2} \quad (3)$$

$\mathrm{x_{inj}}$, $\mathrm{y_{inj}}, \mathrm{z_{inj}}$ and $\mathrm{x_d}$, $\mathrm{y_d}, \mathrm{z_d}$ are the coordinates of the injector tip and the single droplet, respectively.
If $\mathrm{DIST_{inj}} \leq \mathrm{T_d}$, only Stripping regime is enabled. The condition for the latter to take place is reported in Eq. 4: break-up occurs only if droplet diameter is larger than $\mathrm{D_{strip}}$. Droplets for which stripping condition is not satisfied do not undergo break-up between the injector tip and $\mathrm{T_d}$. Characteristic time of break-up is reported in Eq. 5. Both $\mathrm{D_{stripping}}$ and $\tau_{\mathrm{stripping}}$ are inherited from the original Reitz-Diwakar model. It is interesting to point out that Stripping condition expressed by Eq. 4 relies on both Weber and Reynolds numbers, the latter being defined as in Eq. 6. $\mathrm{C_{s1}}$ and $\mathrm{C_{s2}}$ are model parameters. In the original Reitz-Diwakar model the former is equal to 0.5 and the latter ranges from 0.5 to 20. ρ_{d}, $\mathrm{D_d}$, σ_{d} are density, diameter and surface tension of the droplet. ρ_{gas} and μ_{gas} are density and molecular viscosity of the gas.
If $\mathrm{DIST_{inj}} > \mathrm{T_d}$, a Bag-like break-up is assumed. Stable droplet diameter ($\mathrm{D_{bag}}$) and characteristic time of break-up (τ_{bag}) are reported in Eq. 7 and 8, and they are still inherited from the Reitz-Diwakar model. Similarly to Stripping, break-up occurs if drop diameter is larger than the stable one and the formulation of the latter comes from the criterion for Bag onset. $\mathrm{C_{b1}}$ and $\mathrm{C_{b2}}$ are model parameters. In the original Reitz-Diwakar model the former is set to 6 according to Wierzba [44] and the latter is equal to π.
Regardless the mechanism, break-up rate is calculated as in Eq. 9, where stable diameter ($\mathrm{D_{d,stable}}$) and characteristic time of break-up (τ_{b}) can be equal either to $\mathrm{D_{stripping}}$ and $\tau_{\mathrm{stripping}}$ or $\mathrm{D_{bag}}$ and τ_{bag} based on the distance from the injector tip.

$\frac{\mathrm{We_g}}{\sqrt{\mathrm{Re_d}}} \geq \mathrm{C_{s1}} \rightarrow \mathrm{D_d} \geq \frac{4\mathrm{C_{s1}^2}\,\sigma_{\mathrm{d}}^2}{\rho_{\mathrm{gas}}\,\mu_{\mathrm{gas}}\,\mathrm{v_{rel}^3}} = \mathrm{D_{strip}}$ (4)	$\mathrm{We_g} \geq \mathrm{C_{b1}} \rightarrow \mathrm{D_d} \geq \frac{2\,\mathrm{C_{b1}}\,\sigma_{\mathrm{d}}}{\rho_{\mathrm{gas}}\,\mathrm{v_{rel}^2}} = \mathrm{D_{bag}}$ (7)
$\tau_{\mathrm{stripping}} = \frac{\mathrm{C_{s2}}}{2}\left(\frac{\rho_{\mathrm{d}}}{\rho_{\mathrm{gas}}}\right)^{1/2}\frac{\mathrm{D_d}}{\mathrm{v_{rel}}}$ (5)	$\tau_{\mathrm{bag}} = \frac{\mathrm{C_{b2}}\,\rho_{\mathrm{d}}^{1/2}\,\mathrm{D_d^{3/2}}}{4\sigma_{\mathrm{d}}^{1/2}}$ (8)

$$Re_d = \frac{\rho_{gas}\, v_{rel}\, D_d}{\mu_{gas}} \quad (6)$$

$$\frac{dD_d}{dt} = \frac{(D_d - D_{d,stable})}{\tau_b} \quad (9)$$

3 Analysed Injectors and Condition, Numerical Setup

In the present work three single-hole diesel injectors are analysed, namely Spray A, Spray C and Spray D, provided by ECN. All the nozzles are simulated at the same operating condition, characterized by ambient pressure and temperature equal to 6 MPa and 900 K, respectively. The adopted fuel is n-Dodecane. Injection pressure and temperature are equal to 150 MPa and 363 K, respectively. Nozzle diameters and hydraulic coefficients for the injectors are reported in Fig. 1. The Spray C nozzle is manufactured to intentionally produce cavitation within the hole, thus reducing Ca. On the other hand, Spray D nozzle is designed to minimize cavitation and, thus, the difference between the orifice diameter and the effective one.

Spray	A	C	D
Geometrical Diameter [µm]	84	200	186
Discharge Coefficient *Cd*	0.89	0.72	0.92
Area Coefficient *Ca*	0.98	0.87	0.93
Velocity Coefficient *Cv*	0.91	0.82	0.99
Effective Diameter [µm]	83	186	179

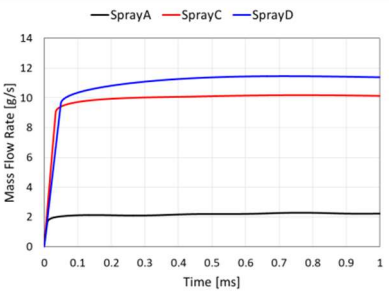

Fig. 1. Nozzle parameters for the three injectors and experimental mass flow rates.

Lagrangian simulations are carried out by means of STAR-CD V2019.1 [45], licensed by Siemens-PLM. Computational domain consists in a cube-shaped vessel whose characteristic dimension is 108 mm for Spray A and 124 mm for both Spray C and Spray D. The numerical grid is reported in Fig. 2 and it consists of hexahedral cells. It includes a refinement, in the spray core region, whose dimensions are reported in Fig. 2. The characteristic cell size in the refinement is 0.5 mm (common for all the injectors). As shown in [46], this value represents the best compromise between a limited computational cost and a reduced mesh dependency. Turbulence is modelled via a Reynolds-Averaged Navier-Stokes (RANS) approach for all the simulations. In particular, the k-ε STANDARD two-equation turbulence model [ref] is adopted for all the injectors. A combined Eulerian-Lagrangian approach is employed to properly represent both the vessel gaseous ambient and the dispersed liquid phase. The second order numerical Monotone Advection and Reconstruction Scheme (MARS) is adopted for momentum, temperature, turbulent quantities and scalars transport equations. Time-step is nearly 1e-7 s to hold the maximum Courant number below unity, while the number of injected parcels per time-step is set equal to 30 for each injector. Computational domain is initialized with experimental pressure and temperature values and, to replicate the experimental quiescent vessel conditions, initial turbulent intensity is set equal to 0 for all the cases. All the boundaries are set as a non-slip adiabatic walls. Properties of the single-component fuel are inherited from the National Institute of Standards and Technology (NIST) database for both the liquid and the vapour phases [47]. Mass flow rate for each injector is provided by the ECN

and it is reported in Fig. 1. The syringe-like effect described in [48] is considered to improve numerical results during the ballistic stage of the injection. The main consequence of this effect is that the initial mass flow rate is characterized by a non-zero value. Atomization is replaced by a blob model and disruption of the big drops (namely blobs) which should replicate the effect of the primary break-up is demanded to the secondary break-up model. Blob initial conditions derive from the hydraulic coefficients provided by ECN. The initial diameter relies on the nozzle effective diameter, which is evaluated from the geometrical one and the area coefficient. Specifically, the initial diameter is imposed via a Rosin-Rammler (RR) distribution whose diameter and exponent are equal to the nozzle effective diameter and 5, respectively. The RR distribution is modified clipping the maximum diameter to the nozzle effective one. As for the initial velocity, it is calculated from the velocity coefficient, which in turn corresponds to the ratio between discharge and area coefficients. Further details on the droplet initialization based on the hydraulic coefficients can be found in [49, 50]. The semi-cone angle is fixed to nearly 5° for all the injectors. As for the secondary break-up, the GruMo model is employed with Cb1 = 1.5, Cb2 = 0.8, Cs1 = 0.5 and Cs2 = 17.5, for all the investigated injectors. For comparison, the widely diffused Reitz-Diwakar model [40, 41] is adopted as well. For the latter, model constants are not modified compared to the reference papers (i.e. Cb1 = 6, Cb2 = 3.14, Cs1 = 0.5 and Cs2 = 20).

Spray	A	C, D
L1 [mm]	8	16
H1 [mm]	20	35
L2 [mm]	30	45
H2 [mm]	40	50

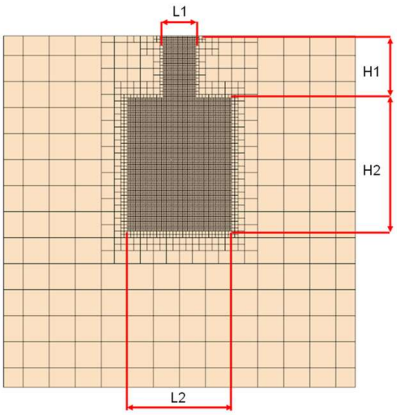

Fig. 2. Numerical grids adopted for the three injectors along with their parameter values.

4 Results

Lagrangian simulations for all the injectors are validated against experimental data in terms of liquid and vapour penetration curves and imaging. Liquid penetration is evaluated as the distance from the tip, along the injector axis, at which the 99% of the injected mass is found [51]. Similarly, vapour penetration is evaluated as the furthest distance at which a vapour concentration of 0.1% is found. A comparison between GruMo and Reitz-Diwakar break-up models is considered for all the injectors.

4.1 Spray A

A first comparison between experimental and numerical data is carried out in terms of liquid and vapour penetrations, as reported in Fig. 3. GruMo break-up model provides a

good representation of the liquid penetration curve in both ballistic and steady stages of the injection, while a slight underestimation of the vapour penetration is noticed. The main reason of such under-prediction is still under investigation. Instead, Reitz-Diwakar break-up model produces liquid and jet penetrations lower than the experimental counterparts, due to the higher break-up rate.

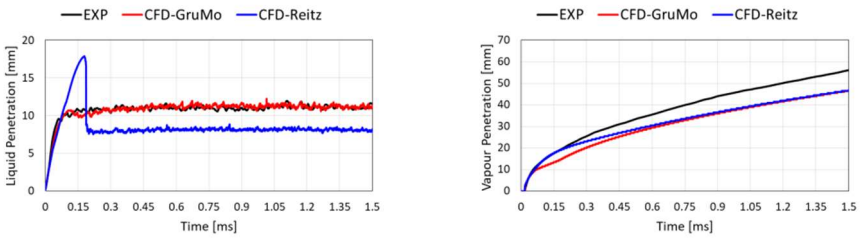

(a) (b)

Fig. 3. Comparison between experimental and numerical data in terms of liquid penetration (a) and vapour penetration (b).

The results are confirmed comparing numerical and experimental outcomes in terms of imaging. Liquid is reported in Fig. 4, while vapour in Fig. 5.

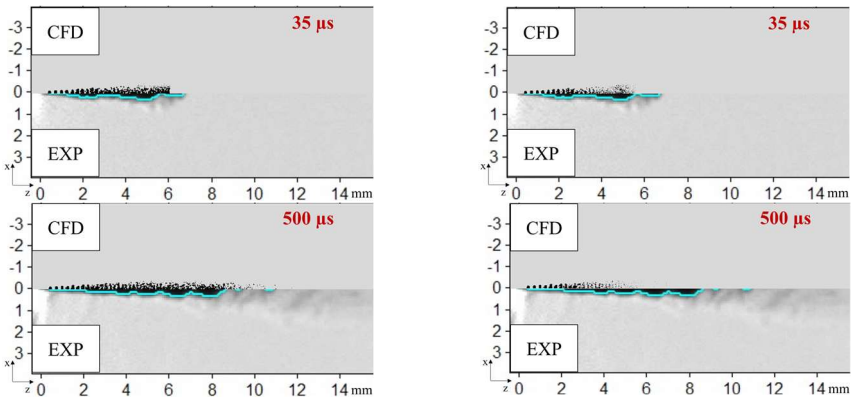

(a) (b)

Fig. 4. Comparison in terms of liquid phase snapshots using (a) the GruMo model, and (b) the Reitz-Diwakar one.

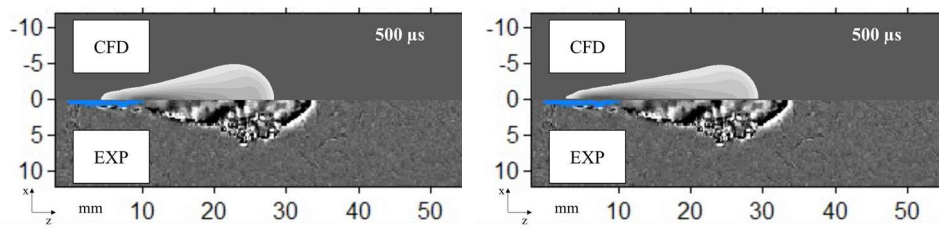

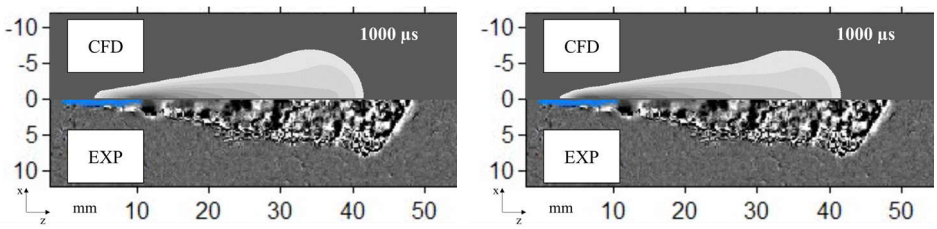

(a) (b)

Fig. 5. Comparison in terms of vapor phase snapshots using (a) the GruMo model and (b) the Reitz-Diwakar one. Experimental images are obtained via the Schlieren technique.

4.2 Spray C and Spray D

In the light of the promising results for the Spray A, the GruMo model is applied to both spray C and Spray D. Liquid and vapour penetration comparisons for both the injectors are reported in Fig. 6. Simulations with the GruMo model show a good agreement between the numerical and experimental liquid penetration curves. It is interesting to notice that the numerical liquid penetration of the Spray D is higher than the Spray C one, as indicated by the experiments. On the contrary, simulations with the Reitz-Diwakar model are characterized by an underestimation of the liquid penetration for both injectors and a negligible difference between the two numerical curves can be noticed. As for the vapour penetration, both GruMo and Reitz-Diwakar models provide an underestimation of the experimental curves of Spray C and Spray D. Numerical and experimental snapshots of the vapour jets are reported in Fig. 7, for both the sprays. As for the liquid, no experimental image is available. The comparison proposed in Fig. 7 visually confirms the results proposed in Fig. 6 in terms of vapour penetration curves.

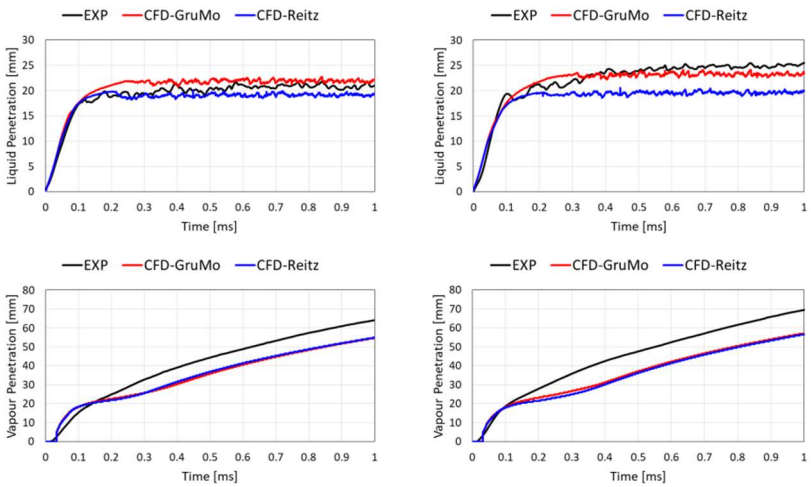

(a) (b)

Fig. 6. Comparison between numerical outcomes and experimental results in terms of liquid (up) and vapour (down) penetrations, for Spray C (a) and Spray D (b).

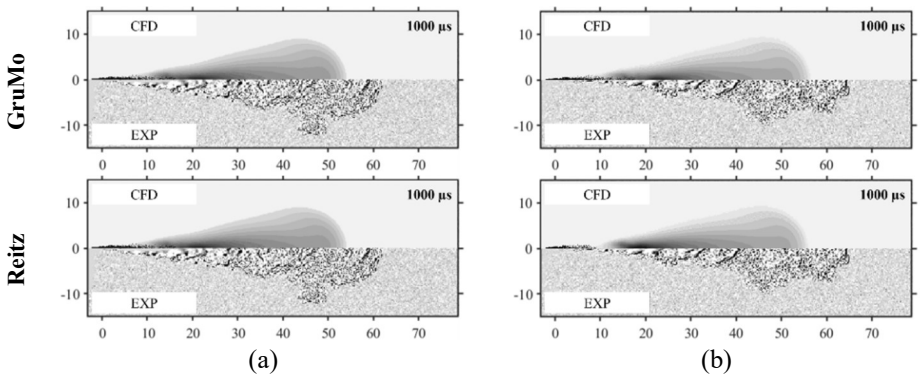

Fig. 7. Effect of the secondary break-up model on the vapor jet, for Spray C (a) and Spray D (b). Experimental images are obtained via the Schlieren technique.

Conclusions

In the present paper, a numerical framework for the 3D-CFD simulation of Diesel sprays is proposed. Attention is mainly focused on the secondary break-up modeling. An alternative break-up model is proposed, which is a modified version of the well-consolidated Reitz-Diwakar one. Compared to the latter, the proposed GruMo model is characterized by a zonalization of the break-up regimes, to speed up the calibration process. Three different injectors provided by the ECN are investigated: Spray A which is representative of injectors for light-duty applications; Spray C and Spray D which are representative of heavy-duty nozzles. Compared to the existing Reitz-Diwakar, the GruMo model provides numerical results in terms of liquid and vapour penetrations and imaging that are much more in agreement with the experimental counterpart, with a unique set of calibration constants, for all the analyzed injectors. The importance of such findings is twofold. On the hand, the proposed model proves to be effective. On the other hand, the adopted numerical framework calibrated on the Spray A (i.e. on a light-duty injector) can be proficiently adopted (at least on equal operating conditions) to simulate heavy-duty nozzles without any further tuning of the models (as demonstrated by the application on Spray C and Spray D).

References

1. Benajes, J., et al., Evaluation of the passive pre-chamber ignition concept for future high compression ratio turbocharged spark-ignition engines. Applied Energy, 2019. **248**: p. 576-588.
2. Paltrinieri, S., et al., Water Injection Contribution to Enabling Stoichiometric Air-to-Fuel Ratio Operation at Rated Power Conditions of a High-Performance DISI Single Cylinder Engine. 2019, SAE International.
3. Lee, J., et al., Bowl Shape Design Optimization for Engine-Out PM Reduction in Heavy Duty Diesel Engine. 2015, SAE International.
4. Mangeruga, V., et al., Design of a Hybrid Power Unit for Formula SAE Application: Packaging Optimization and Thermomechanical Design of the Electric Motor Case. SAE Int. J. Adv. & Curr. Prac. in Mobility, 2019. **2**(2): p. 721-736.
5. Seibel, J., S. Pischinger, and P. von Dincklage, Optimized Layout of Gasoline Engines for Hybrid Powertrains. 2008, The Automotive Research Association of India.
6. Koci, C., et al., A Hybrid Heavy-Duty Diesel Power System for Off-Road Applications - Concept Definition. SAE Technical Paper Series, 2021: p. Medium: ED.
7. Cracknell, R., et al., Assessing the Efficiency of a New Gasoline Compression Ignition (GCI) Concept. 2020, SAE International.

8. Zheng, Z. and M. Yao, Charge stratification to control HCCI: Experiments and CFD modeling with n-heptane as fuel. Fuel, 2009. **88**(2): p. 354-365.
9. D'Adamo, A., et al., Chemistry-Based Laminar Flame Speed Correlations for a Wide Range of Engine Conditions for Iso-Octane, n-Heptane, Toluene and Gasoline Surrogate Fuels. SAE Technical Papers, 2017. **2017-October**.
10. An, Y.-z., et al., Development of a soot particle model with PAHs as precursors through simulations and experiments. Fuel, 2016. **179**: p. 246-257.
11. Del Pecchia, M., et al., A threshold soot index-based fuel surrogate formulation methodology to mimic sooting tendency of real fuels in 3D-CFD simulations. Applied Energy, 2020. **280**: p. 115909.
12. Del Pecchia, M., et al., Gasoline-ethanol blend formulation to mimic laminar flame speed and auto-ignition quality in automotive engines. Fuel, 2020. **264**.
13. Bozza, F., et al., Refinement of a 0D Turbulence Model to Predict Tumble and Turbulent Intensity in SI Engines. Part I: 3D Analyses. SAE Technical Papers, 2018. **2018-April**.
14. Bozza, F., et al., Refinement of a 0D Turbulence Model to Predict Tumble and Turbulent Intensity in SI Engines. Part II: Model Concept, Validation and Discussion. 2018, SAE International.
15. De Bellis, V., et al., Development of a phenomenological turbulence model through a hierarchical 1D/3D approach applied to a VVA turbocharged engine. SAE International Journal of Engines, 2016. **9**(1): p. 506-519.
16. Millo, F., C.V. Ferraro, and L. Pilo, A Contribution to Engine and Vehicle Performance Prediction. 2000, SAE International.
17. D'Adamo, A., et al., Development of a RANS-Based Knock Model to Infer the Knock Probability in a Research Spark-Ignition Engine. SAE International Journal of Engines, 2017. **10**(3).
18. d'Adamo, A., et al., The potential of statistical RANS to predict knock tendency: Comparison with LES and experiments on a spark-ignition engine. Applied Energy, 2019. **249**: p. 126-142.
19. Berni, F., et al., Towards grid-independent 3D-CFD wall-function-based heat transfer models for complex industrial flows with focus on in-cylinder simulations. Applied Thermal Engineering, 2021. **190**: p. 116838.
20. Berni, F., et al., On the existence of universal wall functions in in-cylinder simulations using a low-Reynolds RANS turbulence model. AIP Conference Proceedings, 2019. **2191**(1): p. 020019.
21. Berni, F. and S. Fontanesi, A 3D-CFD methodology to investigate boundary layers and assess the applicability of wall functions in actual industrial problems: A focus on in-cylinder simulations. Applied Thermal Engineering, 2020. **174**.
22. Rosetti, A., et al., CFD analysis and knock prediction into crevices of piston to liner fireland of an high performance ICE. SAE Technical Papers, 2019. **2019**.
23. D'Adamo, A., et al., Understanding the origin of cycle-to-cycle variation using large-eddy simulation: Similarities and differences between a homogeneous low-revving speed research engine and a production DI turbocharged engine. SAE International Journal of Engines, 2018. **12**(1): p. 1-22.
24. Iacovano, C., et al., A Preliminary 1D-3D Analysis of the Darmstadt Research Engine Under Motored Condition. E3S Web Conf., 2020. **197**: p. 06006.
25. Insuk, K., et al. Society of Automotive Engineers technical paper series. 2017, Warrendale, Penn.: Society of Automotive Engineers.
26. Krastev, V.K., et al., Validation of a zonal hybrid URANS/LES turbulence modeling method for multi-cycle engine flow simulation. International Journal of Engine Research, 2019.
27. Rulli, F., et al., A critical review of flow field analysis methods involving proper orthogonal decomposition and quadruple proper orthogonal decomposition for internal combustion engines. International Journal of Engine Research, 2021. **22**(1): p. 222-242.
28. Teodosio, L., et al., Impact of intake valve strategies on fuel consumption and knock tendency of a spark ignition engine. Applied Energy, 2018. **216**: p. 91-104.
29. Chiodi, M., et al., Development of an Innovative Combustion Process: Spark-Assisted Compression Ignition. SAE Int. J. Engines, 2017. **10**(5): p. 2486-2499.

30. Hua, J., et al., Influence of pre-chamber structure and injection parameters on engine performance and combustion characteristics in a turbulent jet ignition (TJI) engine. Fuel, 2021. **283**: p. 119236.
31. Berni, F., et al., Numerical Investigation on the Effects of Water/Methanol Injection as Knock Suppressor to Increase the Fuel Efficiency of a Highly Downsized GDI Engine. SAE Technical Papers, 2015. **2015-September**(September).
32. Berni, F., et al. A numerical investigation on the potentials of water injection to increase knock resistance and reduce fuel consumption in highly downsized GDI engines. in Energy Procedia. 2015.
33. Breda, S., et al. Effects on knock intensity and specific fuel consumption of port water/methanol injection in a turbocharged GDI engine: Comparative analysis. in Energy Procedia. 2015.
34. Teodosio, L., F. Bozza, and F. Berni, Effects of nanofluid contaminated coolant on the performance of a spark ignition engine. AIP Conference Proceedings, 2019. **2191**(1): p. 020147.
35. Assanis, D.N., et al., The Effects of Ceramic Coatings on Diesel Engine Performance and Exhaust Emissions. 1991, SAE International.
36. Rajamani, V.K., S. Schoenfeld, and A. Dhongde, Parametric Analysis of Piston Bowl Geometry and Injection Nozzle Configuration using 3D CFD and DoE. 2012, SAE International.
37. Breda, S., et al., Experimental and numerical study on the adoption of split injection strategies to improve air-butanol mixture formation in a DISI optical engine. Fuel, 2019: p. 104-124.
38. Severi, E., et al. Numerical investigation on the effects of bore reduction in a high performance turbocharged GDI engine. 3D investigation of knock tendency. in Energy Procedia. 2015.
39. Saha, K., Agarwal, A., Ghosh, K., Som, S, Two-Phase Flow for Automotive and Power Generation Sectors. 2019.
40. Reitz, R.D. and R. Diwakar, Effect of Drop Breakup on Fuel Sprays. 1986, SAE International.
41. Reitz, R.D. and R. Diwakar, Structure of High-Pressure Fuel Sprays. 1987, SAE International.
42. Pilch, M. and C.A. Erdman, Use of breakup time data and velocity history data to predict the maximum size of stable fragments for acceleration-induced breakup of a liquid drop. International Journal of Multiphase Flow, 1987. **13**(6): p. 741-757.
43. C., B., Mixture Formation in Internal Combustion Engines. 2006: Springer.
44. Wierzba, A., Deformation and breakup of liquid drops in a gas stream at nearly critical Weber numbers. Experiments in Fluids, 1990. **9**(1): p. 59-64.
45. SIEMENS, STAR-CD METHODOLOGY Version 2019.1. 2019.
46. Sparacino, S., et al., Impact of the primary break-up strategy on the morphology of GDI sprays in 3D-CFD simulations of multi-hole injectors. Energies, 2019. **12**(15).
47. Linstrom, P. and W. Mallard, - The NIST Chemistry WebBook: A Chemical Data Resource on the Internet.
48. Postrioti, L., et al., Experimental and Numerical Analysis of Spray Evolution, Hydraulics and Atomization for a 60 MPa Injection Pressure GDI System. SAE Technical Papers, 2018. **2018-April**.
49. Sparacino, S., et al. Impact of different droplets size distribution on the morphology of GDI sprays: Application to multi-hole injectors. in AIP Conference Proceedings. 2019.
50. Sparacino, S., et al., 3D-CFD Simulation of a GDI Injector Under Standard and Flashing Conditions. E3S Web Conf., 2020. **197**: p. 06002.
51. Sim, J., et al., Spray Modeling for Outwardly-Opening Hollow-Cone Injector. 2016.